THE JOURNAL OF PHYSICAL CHEMISTRY B

Article

pubs.acs.org/JPCB

QM/MM Molecular Dynamics Study of Purine-Specific Nucleoside Hydrolase

Ruibo Wu,[†,‡,§] Wengjin Gong,[§] Ting, Liu,[‡] Yingkai Zhang,[§] and Zexing Cao*[,‡]

[†]School of Pharmaceutical Sciences, East Campus, Sun Yat-sen University, Guangzhou 510006, China

[‡]State Key Laboratory of Physical Chemistry of Solid Surfaces and Fujian Provincial Key Laboratory of Theoretical and Computational Chemistry, College of Chemistry and Chemical Engineering, Xiamen University, Xiamen 361005, China

[§]Department of Chemistry, New York University, New York, New York 10003, United States

ABSTRACT: Although various *T. vivax* purine-specific inosine−adenosine−guanosine nucleoside hydrolase (IAG-NH) crystal structures were determined in recent years, the mechanistic details for the cleavage of *N*-glycosidic bond and the release of base are still unclear. Herein, the irreversible hydrolysis reaction has been studied by ab initio QM/MM MD simulations, and the results indicate a highly dissociative and concerted mechanism. The protonation of substrate at N7 of inosine is found to strongly facilitate the hydrolysis process, while the hydrolysis reaction is less sensitive to the protonation state of Asp 40 residue. The proton-transfer channel and the dependence of activity on the anti/syn-conformation of substrate are also explored.

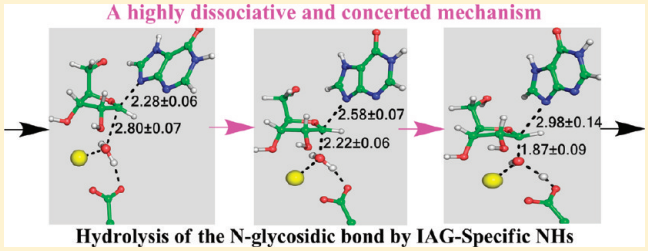

INTRODUCTION

The calcium-dependent nucleoside hydrolases (NHs)[1−7] catalyze the irreversible hydrolysis of the *N*-glycosidic bond (such as the C1′−N9 bond shown in Figure 1a) of ribonucleosides and then release the resulting free purine or pyrimidine base and ribose.[8−10] They are key enzymes in the purine salvage pathway of many pathogenic organisms and have been studied extensively in recent years as potential targets for antiparasitic drug design.[11−16]

According to the difference in substrate specificity, the NHs have been classified into the four distinct subclasses:[17] the nonspecific inosine−uridine nucleoside hydrolase (IU-NH);[18−20] the purine-specific inosine−adenosine−guanosine nucleoside hydrolase (IAG-NH);[8,10,21,22] the pyrimidine-specific cytidine−uridine nucleoside hydrolase (CU-NH);[5,23−25] and the 6-oxo-purine-specific inosine−guanosine nucleoside hydrolase (IG-NH).[26,27] As shown in Figure 1a, the substrates inosine, adenosine, and guanosine are quite similar structurally, the important differences appear in the side group of the 6-membered ring. On the basis of sequence characterization of NHs, they also have been classified into three homology-based groups, where IU-NHs and CU-NHs belong to group I, IAG-NH to group II, and a yet uncharacterized family, group III.[1]

Regarding the quaternary structure of NHs, they probably prefer to crystallize as homotetramer for IU-NH, while the homodimer complex (see Figure 2a) is much more popular for IAG-NH.[1] Recently, a number of *T. vivax* IAG-NHs crystal structures have been determined, including the apo-state (PDB ID: 1HOZ),[8] the wild-type enzyme inhibitor (EI) complex (PDB ID: 1HP0, 3EPW, 3EPX, 2FF1, and 2FF2),[8,16,21] the mutant enzyme−substrate (ES) complex (PDB ID: 1KIC),[10] and the mutant EI complex (PDB ID: 1KIE, 1R4F, and 3B9G).[10,28,29] The anti-conformation of base (as shown in Figure 2b) was the most popular state observed in available crystal structures,[10,16,21,29] but the syn-conformation (as shown in Figure 2b) also exists.[8]

On the basis of experimental thermodynamic and kinetic studies,[10,21,28,30−32] the hydrolysis pathway catalyzed by IAG-NH is considered to be a four-step kinetic model as shown in Figure 1b,[7,28−30,32,33] including substrate binding, chemical reaction, base release, and ribose release. The ribose release is believed to be the rate-determining step, and the rate of product (base and ribose) release is related to a flexible loop (loop 2, residues 244−258) based on the loop deletion mutagenesis analysis.[29] However, the chemical step (cleavage of N−C bond) has been found to be irreversible[7] and very facile.[16,29,32] In most studies, it is suggested that the leaving of base and the nucleophilic attack of water tread the borderline between the concerted and stepwise reactions, via a S_N2-like mechanisms with a so-called oxocarbenium ion-like transition state.[1,29,34] As illustrated in Figure 1a, the leaving group (base) has been suggested to be activated through protonating the N7 site by both experimental and theoretical studies.[1,7,35] The Ca^{2+}-bound water has been thought to be the potential nucleophile to attack the C1′ site. Meanwhile, due to the importance of understanding the breakage of the *N*-glycosidic bond, the first-principles calculations on various gas phase/

Received: November 27, 2011
Revised: January 14, 2012
Published: January 18, 2012

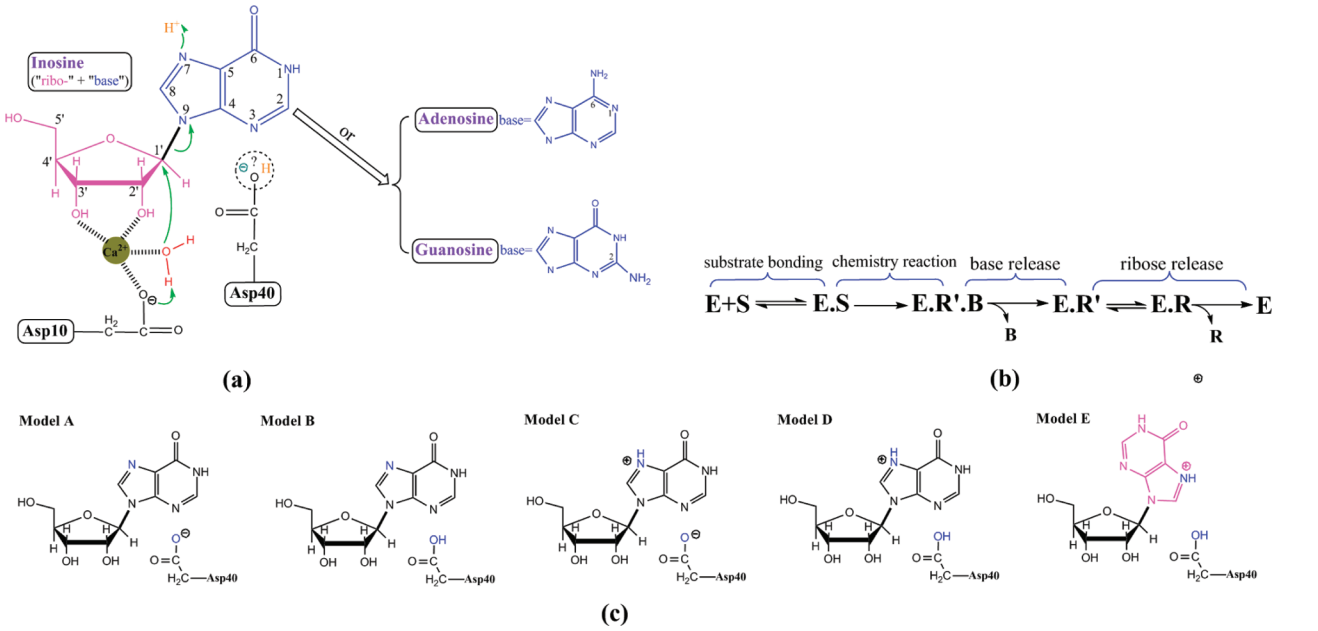

Figure 1. (a) IAG substrates and key residues around the substrate in IAG-NH. (b) The previous suggested four-step kinetic model for IAG-NH. (E, enzyme; S, substrate; R′, bound ribose; R, dissociative ribose; B, base). (c) The five computational models using different prontonated states of *anti*/*syn*-inosine substrate and Asp 40 residue.

solvent models[35−45] and the classical molecular dynamics (MD) simulations[46,47] on the selected enzyme complexes had also been performed.

Despite these extensive studies, however, some basic details of the hydrolytic pathway catalyzed by IAN-GH remain unclear, and many questions are still open, such as (1) where does the proton on N7 come from? How does it promote the breakage of the *N*-glycosidic bond? (2) Which conformation (syn-/anti-) of the substrate is favorable for the hydrolysis reaction? Is there any conformational conversion before chemistry step or not? (3) What's the protonation state of the Asp 40 residue? Is that a key factor that would affect the catalytic activity?

The available crystal structures of IAG-NH only present the static spatial arrangement of heavy atoms in protein complex, and the key residues in loop 2 were missed in most of the crystal structures. Considering the dynamics of protein environment always plays a critical role in the function of protein, herein the MD simulations with combined quantum mechanics and molecular mechanics (QM/MM) potential have been performed to explore the unclear issues in IAG-NH enzyme as mentioned above. The MD simulations at the atomic level would provide insights and correlations among the structures, dynamics, and functions of enzyme. In the QM/MM model, the key residues and the substrates in the active site of the enzyme, which are directly involved in the breaking/formation of a C−N bond, are treated at the QM level. The rest of the protein and solvent is described by the atomic force fields at the MM level to effectively evaluate effects of the fluctuating protein and solvent environment. As this QM/MM strategy combines the accuracy of QM methods and the computational efficiency of MM approach, it has been extensively applied to study enzymatic reactions.[48−59]

■ COMPUTATIONAL DETAIL

Preparation of the IAG-NH Models. Since loop 2 has not been modeled in most of the available XRD structures of *T.vivax* IAG-NH,[8,10,21,28,29] our initial enzyme−substrate models are prepared based on the crystal structure of the EI complex at 1.3 Å resolution (PDB ID: 3EPW[16]) in which the loop 2 residues are included. As shown in Figure 2a, its accessible surface area buried in the dimer interface is very large (∼1297 Å^2),[16] so both chains were kept in the initial model. The inhibitor was modified into the protonated and neutral anti-conformation inosine substrate; the syn-conformation of the substrate was also considered. The previous experiments[10] observed that the optimum solution environment is near pH = 5.0 for IAG-NHs from *T. vivax* using inosine as a substrate; herein, the protonation states of charged residues were determined at pH = 5.0 by the PDB2PQR program.[60] Particularly, both protonated (Ash) and negative (Asp) states of the Asp 40 residue were considered here. As a result, we totally prepared five IAG-NH complexes (shown in Figure 1c): Model A, anti·neutral·Asp40; Model B, anti·neutral·Ash40; Model C, anti·protonated·Asp40; Model D, anti·protonated·Ash40; Model E, syn·protonated·Ash40. Each prepared system was solvated into a ∼90 × 80 × 120 Å rectangular water box with an 8 Å buffer distance between the solvent box wall and the nearest solute atom. Finally, several sodium ions were added at the protein surface to neutralize each model system, and the resulting system has a total of about 71 800 atoms.

For each of the five model systems, followed by a multistep minimization and MD equilibration protocol, more than 3 ns NVT MD simulations at 300 K were carried out via employing the periodic boundary condition. The Berendsen thermostat method[61] was used to control the system temperature. All MD simulations were performed with AMBER10 molecular dynamics package.[53] The Amber99SB force field[62−64] for the protein and TIP3P model[65] for water molecules were employed. The force field parameters for the substrates in each model were generated from AMBER GAFF force field,[66] and the partial atomic charge of substrate was assigned by the restrained electrostatic potential (RESP) charge from HF/6-31G* calculation with Gaussian03 package.[67] During MD

dx.doi.org/10.1021/jp211403j | J. Phys. Chem. B 2012, 116, 1984−1991

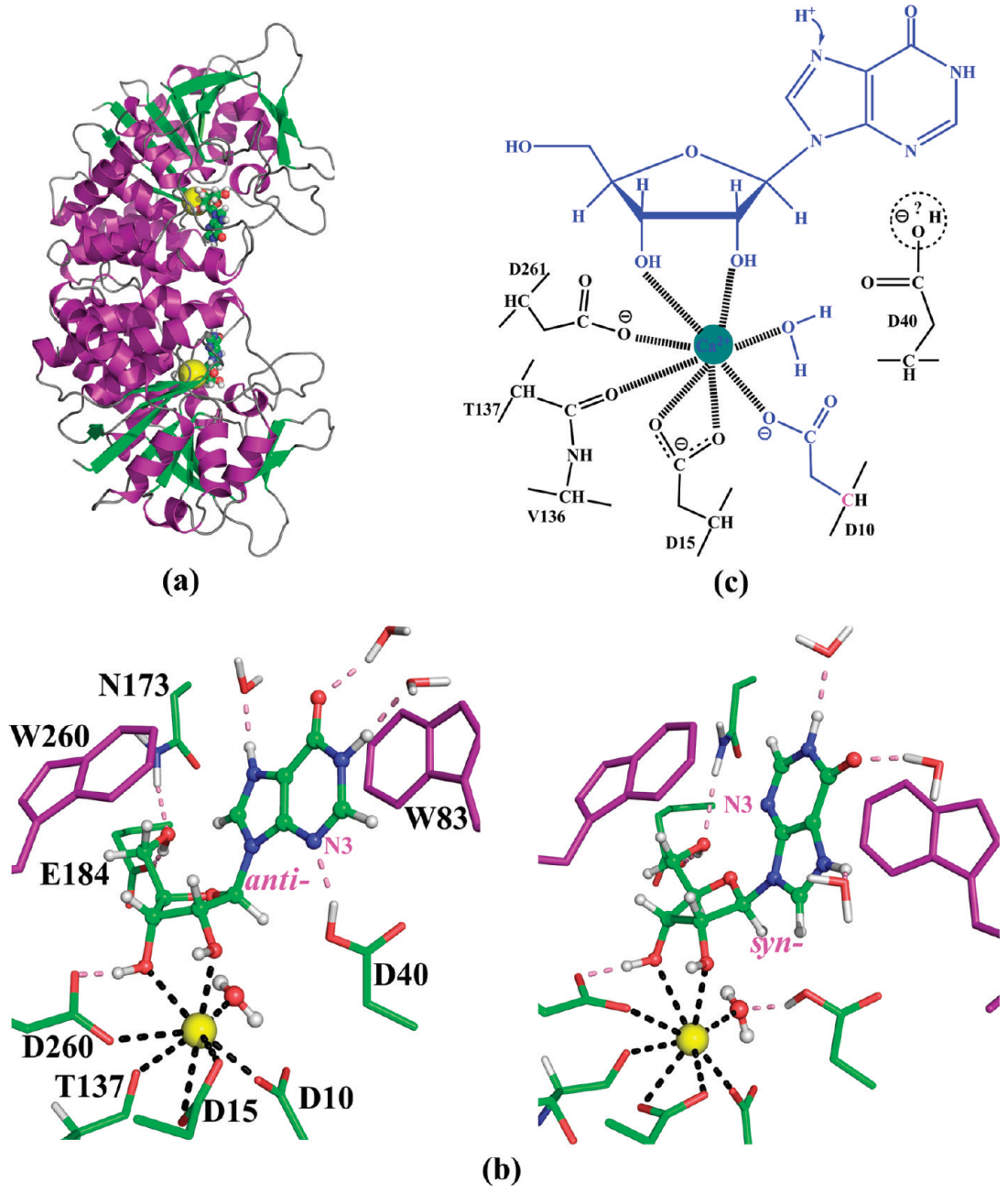

Figure 2. (a) Secondary structure of IAG NH. (b) The active-site structure around the anti-substrate in Model D and the syn-substrate in Model E from the MM MD trajectory (last snapshot). (c) The QM/MM partition for the QM/MM computational models. The QM atoms are colored in blue, and the pseudo atom is colored in pink.

simulations, the SHAKE algorithm[68] was utilized to constrain all bonds involving hydrogen atoms with tolerance of 10^{-5}, and a time step of 2 fs was set. The 12 Å cutoff was employed for both van der Waals and electrostatic interactions. The final snapshot from the stable trajectory was used to prepare for subsequent QM/MM studies.

QM/MM MD Simulations. Each QM/MM model was prepared by deleting the solvent molecules beyond 30 Å from the N9 atom. The resulting QM/MM system consists of ~22 000 atoms. The detailed QM/MM partition for all these models are presented in Figure 2c. The QM subsystem, which includes Asp10, calcium ion, Ca^{2+}-bound water, and substrate, are treated with the B3LYP functional using the 6-31G(d) basis set. The QM/MM boundary was described by the improved pseudobond approach.[69−71] The other atoms were described by the same molecular mechanical force field used in classical MD simulations. The spherical boundary condition was applied and the atoms more than 23 Å away from the spherical center were fixed. The 18 and 12 Å cutoffs were employed for electrostatic and van der Waals interactions respectively. There was no cutoff for electrostatic interactions between QM and MM regions.

To characterize the chemistry step, the QM/MM minimization calculation was employed to map out a minimum energy path with the reaction coordinate driving method,[72] and $d_{C1'\text{-}N9}-d_{C1'\text{-}Ow}-d_{Hw\text{-}OD2}$ was chosen as the reaction coordinate for all of the five models. For all of the determined structures along the reaction path of Models D and E, their MM

dx.doi.org/10.1021/jp211403j | J. Phys. Chem. B 2012, 116, 1984−1991

subsystems were further equilibrated by molecular mechanical MD simulations for 500 ps with the frozen QM subsystem. Then, the resulting snapshots were used as starting structures for ab initio QM/MM MD simulations with umbrella sampling. Each window was simulated for 25 ps with 1 fs time step at the QM(B3LYP/6-31G*)/MM level. The configurations from the last 20 ps trajectory for each window were collected for data analysis. The probability distributions along the reaction coordinate were determined for each window and pieced together with the WHAM[73,74] to calculate the free energy profile. The Beeman algorithm[75] was used to integrate the Newton equations of motion, and the Berendsen thermostat method[61] was employed to control the system temperature at 300 K. All our ab initio QM/MM calculations were performed with modified Q-Chem[76] and Tinker[77] programs.

RESULTS AND DISCUSSION

Protonation State of Asp 40/Substrate and Catalytic Mechanism of *T.vivax* IAG-NH. First, we determined the minimal energy path (MEP) of the catalytic reaction step for Models A–D with B3LYP(6-31G*) QM/MM calculations, as shown in Figure 3. The reaction barrier is ~10.0 kcal/mol for the protonated substrate at the N7 site (Models C and D), much lower than ~34.0 kcal/mol for the neutral substrate (Models A and B). Thus, our results support that the substrate should be protonated at N7. However, the protonation state of Asp 40 has almost no effect on the hydrolysis reaction as shown in Figure 3. We also found that a stable hydrogen bond was formed directly between N3 with Ash 40 in Model D, and a stable hydrogen bond was observed between a water molecular and N3 atom in Model C.

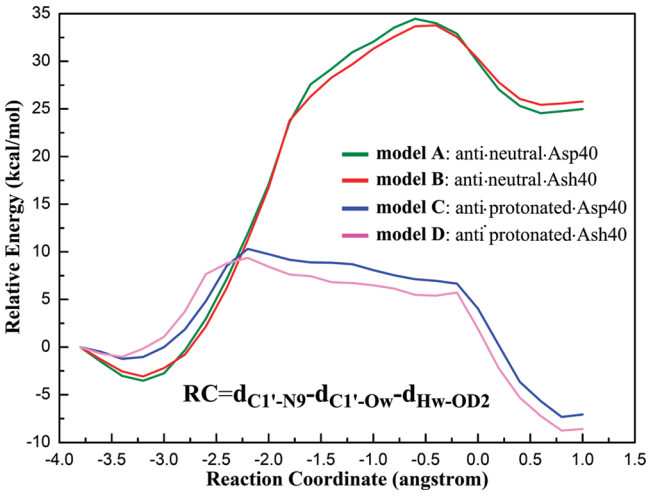

Figure 3. Relative energy profiles along the defined reaction coordinate for various computational models.

Then for Model D, we have carried out ab initio QM/MM MD simulations and umbrella sampling to determine its free energy profile. Since both A and B chains of the enzyme were kept in our computational models, either the active site in chain A or that in chain B could be considered as the QM part (in sphere center). Thus, we determined two free energy profiles, as shown in Figure 4. We can see that free energy profiles are very consistent between two choices of the QM subsystem, which indicates that our QM/MM simulation protocol is quite robust. The calculated free energy barrier is ~7.0 kcal/mol, and the product state is ~10.5 kcal/mol lower than the reaction state, which is consistent with experimental observation that the cleavage of N–C bond is irreversible[7] and very facile.[16,29,32] The QM/MM-optimized geometries of the active site in chain B as the QM part along the reaction coordinate were also shown in Figure 4. At the reactant state, the water molecule, ~3.2 Å away from C1′, forms a hydrogen bond with Asp 10. First, N9 leaves C1′ (the distance between N9 and C1 increases very fast from ~1.5 Å to ~2.3 Å) quickly, and then H_2O slowly approaches the C1′ site to produce an oxocarbenium-ion-like transition state. The dihedral angles shown in Figure 4 indicate that C1′ is a sp^3-type carbon at the reactant state, while it becomes sp^2 hybridized at the transition state. Then, the base leaves away from the ribose group, and the oxygen of water attacks the C1′ atom by degrees (from R_c = −2.2 Å to R_c = 0.0 Å). Finally, the hydroxyl group bonds to C1′ coupled with one proton transfer to Asp 10, yielding the dissociative base via a complete breakage of the *N*-glycosidic bond. Therefore, our

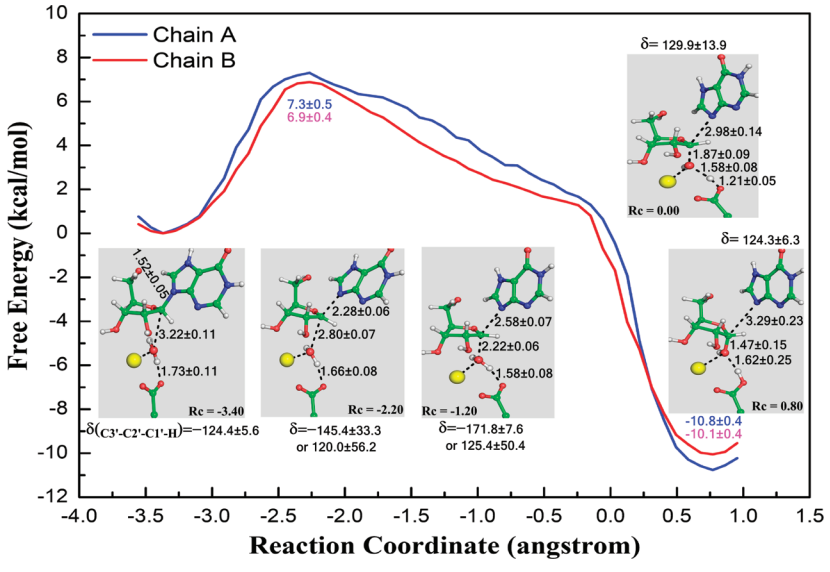

Figure 4. Free energy profiles and the active-site structures along the hydrolysis reaction for Model D.

dx.doi.org/10.1021/jp211403j | J. Phys. Chem. B 2012, 116, 1984–1991

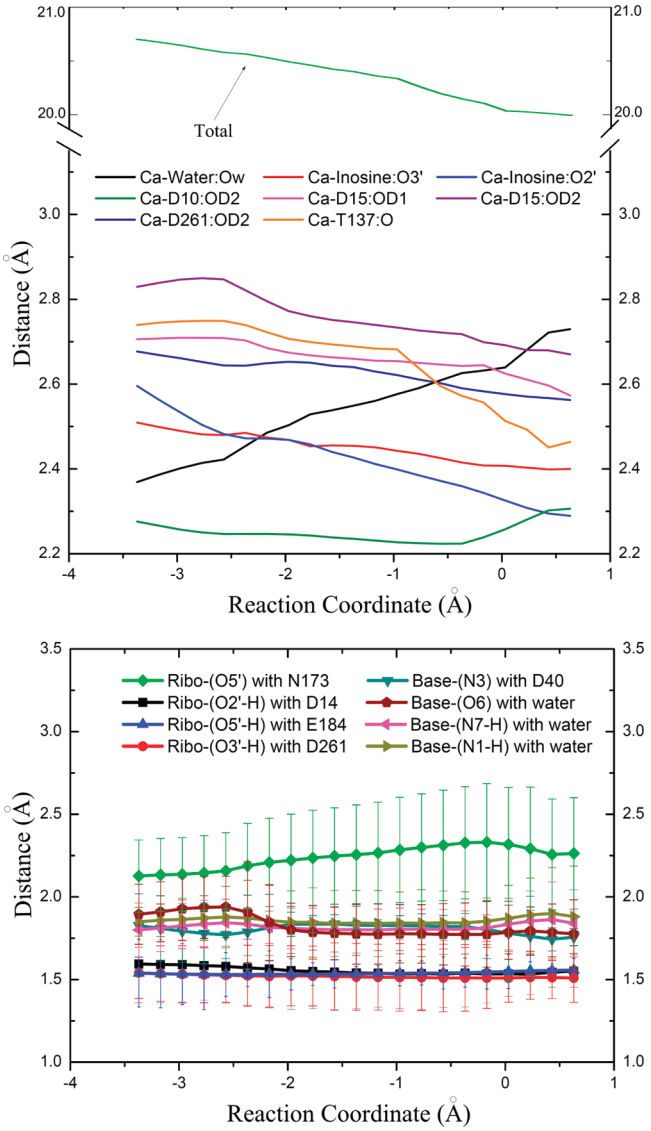

Figure 5. Coordination bond distances from Ca^{2+} (total means the summary of all coordination bonds length) and the direct hydrogen bond around the ribo and base groups along the reaction coordinate.

QM/MM simulations support a highly dissociative and concerted mechanism for the hydrolysis reaction. Such a similar mechanism has also recently been characterized for the *N*-glycosidic bond cleavage reaction catalyzed by sirtuins.[48,78−81]

Interactions in the Ribose/Base Binding Pocket. For Model D, we have calculated the coordination bond distances of the calcium coordination shell and the hydrogen bond around the ribo and base groups along the reaction coordinate. As shown in Figure 5, at the reactant state, the calcium cation is ligated by eight oxygen atoms from Asp 10, Asp15 (bidentate), Thr 137, Asp 261, H_2O, and the ribose (bidentate), and approximately constitutes a hexahedral geometry. Interestingly, although the water molecule moves away from Ca^{2+} gradually along the hydrolysis reaction pathway (see Figure 5), the average coordination distance of all ligand atoms to Ca^{2+} keeps decreasing (~2.59 Å at the reactant state and ~2.49 Å at the product state by average). This indicates that its interactions with other ligands such as inosine, Asp15, Asp261, and Thr137 become much stronger as the reaction proceeds.

As shown in Figure 6, the hydrogen bond network around the base and ribose, linking either the amino acid residues or water molecules, is very complicated, and these hydrogen bonds are very stable along the reaction coordinate. Especially, the hydrogen atoms on O2′, O3′, and O5′ form very short hydrogen bonds with an average distance of 1.5 Å. As proposed in previous gas phase QM studies, hydrogen bonding interactions around the base can cooperate together to facilitate the cleavage of the *N*-glycosidic bond. In our QM/MM condensed model, we note that the hydrogen bond between N7−H and the solvent water molecule is formed at the reactant state, and it extends to the outer solvent environment through a water chain, which might be an efficient pathway to protonate the substrate (vide infra).

In addition, we have compared the hydrogen bond networks around the N7 site in Models B/D/E. As shown in Figure 6, a stable water chain channel was always observed to connect N7 to the bulk solvent by hydrogen bond interactions in all of models, and the previous study on the transition-state complex of the IAG-NH also proposed the presence of a water channel and its involvement in catalysis.[21] Meanwhile, considering that the stacking interactions of the parallel aromatic rings from Trp260 and Trp83 could raise the pK_a value of the N7 site as shown in previous computational and experimental studies, it can be expected that this water chain would be an efficient channel for the proton transfer from the outer water solvent to the N7 atom. Meanwhile, the nucleophile water is activated by interacting with the Ca^{2+} cation as well as forming a hydrogen bond with the Asp10. As a result, the water is favorable to release a proton.

Structure and Kinetic Comparison between Anti- and Syn- Substrates. As both anti- and syn-conformation substrates have been observed in crystal structures, it would be interesting to compare the structural features of the active site and the kinetic properties of the hydrolysis reaction. Thus, we have carried out simulations of Model E, in which the substrate is in syn-conformation.

As shown in Figure 6d, although the N7 site is buried more deeply in the active site for the syn-conformation substrate, compared to its anti-conformation counterpart, a potential proton transfer channel also exists. Therefore, N7 could be efficiently protonated in the syn-substrate−enzyme complex. The free energy profile and the active-site geometry along the reaction coordinate for Model E are shown in Figure 7. We can see that the hydrolysis is also an irreversible thermodynamic process with reaction ΔG of ~−8.6 kcal/mol and a low free energy barrier of ~9.0 kcal/mol. Since the reaction barrier for the further evolution of hydrolysis from the intermediate configuration to the product state is only ~1.4 kcal/mol, the hydrolysis reaction may be viewed as either a concerted or stepwise process. The comparable relative free profiles for the hydrolysis reaction of the anti- and syn-conformations do not lend support to that the transformation from the syn-conformation to the anti-conformation is requisite for the hydrolysis reaction proposed in a previous study.[46]

■ CONCLUSIONS

By employing ab initio QM/MM MD simulations of various inosine-NH models, the irreversible hydrolysis reaction catalyzed by IAG-NH has been suggested to employ a highly dissociative and concerted mechanism. A stable hydrogen bond network connecting the N7 atom and the outer solvent water has been observed, which would protonate N7 of the substrate

dx.doi.org/10.1021/jp211403j | J. Phys. Chem. B 2012, 116, 1984−1991

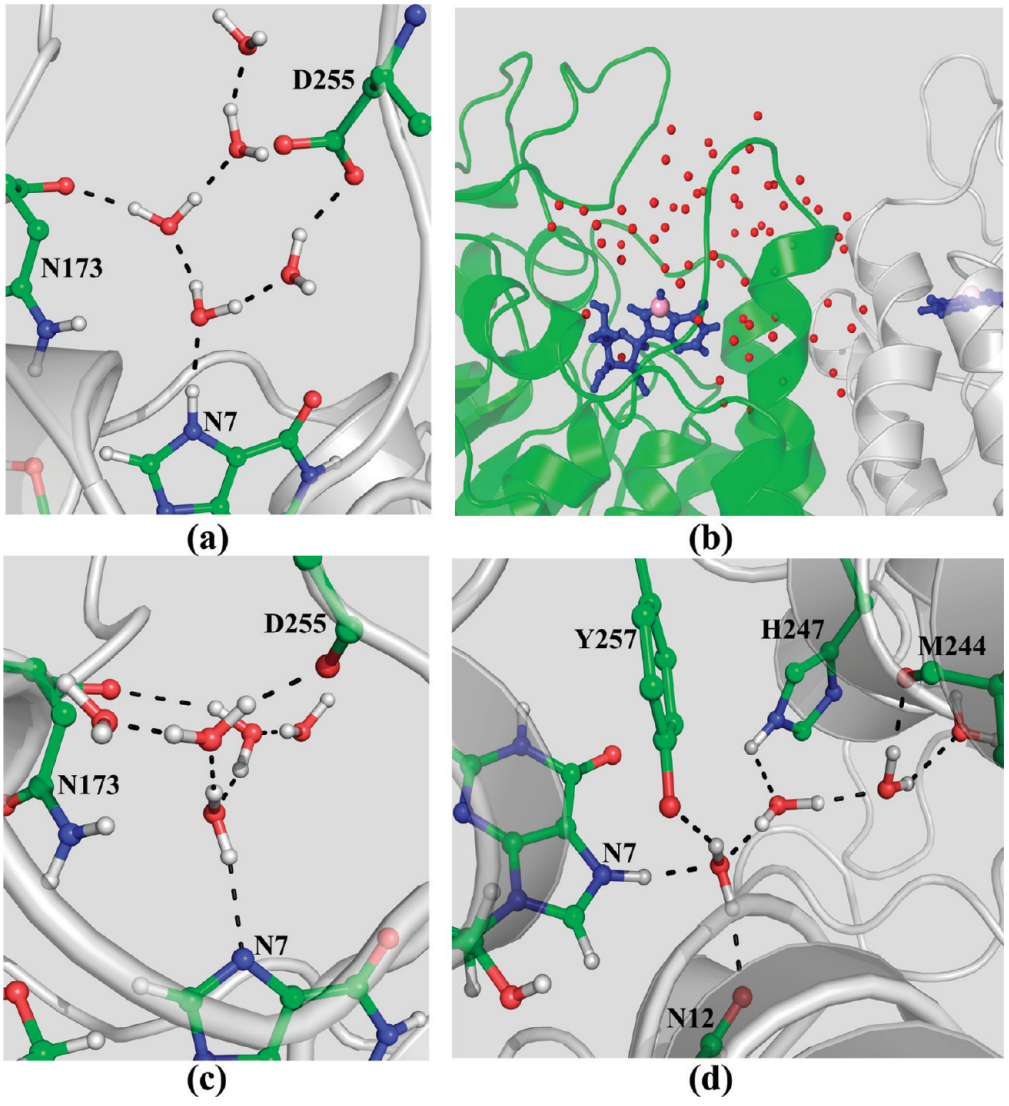

Figure 6. Hydrogen bond network around the N7 site in Model D (a,b), Model B (c), and Model E (d).

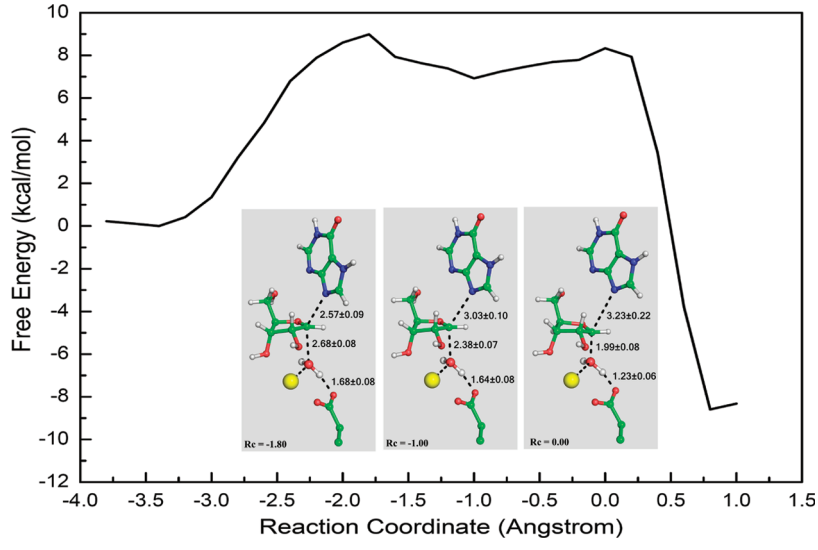

Figure 7. Free energy profiles and the active-site structures along the hydrolysis reaction for Model E.

at acidic conditions. Our simulation results indicate that the substrate protonation at N7 plays an important role to promote the bond cleavage of C1′–N9. However, the protonation state of the Asp 40 residue has little effect on the hydrolysis reaction,

dx.doi.org/10.1021/jp211403j | J. Phys. Chem. B 2012, 116, 1984–1991

and the kinetic difference of the anti/syn-conformations of the substrate is quite small: the anti-comformation is a preferred substrate state, but the syn-conformation of inosine has a comparable activity.

AUTHOR INFORMATION

Corresponding Author

*E-mail: zxcao@xmu.edu.cn.

Notes

The authors declare no competing financial interest.

ACKNOWLEDGMENTS

This work was supported by the Ministry of Science and Technology (2011CB808504 and 2012CB214902) and the National Science Foundation of China (21133007 and 20873105). We thank NYU-ITS for providing computational resources.

REFERENCES

(1) Versees, W.; Steyaert, J. *Curr. Opin. Struct. Biol.* **2003**, *13*, 731−738.

(2) Versees, W.; Van Holsbeke, E.; De Vos, S.; Decanniere, K.; Zegers, I.; Steyaert, J. *Acta Crystallogr., Sect D: Biol. Crystallogr.* **2003**, *59*, 1087−1089.

(3) Petersen, C.; Moller, L. B. *J. Biol. Chem.* **2001**, *276*, 884−894.

(4) Cui, L. W.; Rajasekariah, G. R.; Martin, S. K. *Gene* **2001**, *280*, 153−162.

(5) Kurtz, J. E.; Exinger, F.; Erbs, P.; Jund, R. *Curr. Genet.* **2002**, *41*, 132−141.

(6) Ribeiro, J. M. C.; Valenzuela, J. G. *Insect Biochem. Mol. Biol.* **2003**, *33*, 13−22.

(7) Berti, P. J.; McCann, J. A. B. *Chem. Rev.* **2006**, *106*, 506−555.

(8) Versees, W.; Decanniere, K.; Pelle, R.; Depoorter, J.; Brosens, E.; Parkin, D. W.; Steyaert, J. *J. Mol. Biol.* **2001**, *307*, 1363−1379.

(9) Porcelli, M.; Peiluso, I.; Marabotti, A.; Facchiano, A.; Cacciapuoti, G. *Arch. Biochem. Biophys.* **2009**, *483*, 55−65.

(10) Versees, W.; Decanniere, K.; Van Holsbeke, E.; Devroede, N.; Steyaert, J. *J. Biol. Chem.* **2002**, *277*, 15938−15946.

(11) Berg, M.; Bal, G.; Goeminne, A.; Van der Veken, P.; Versees, W.; Steyaert, J.; Haemers, A.; Augustyns, K. *ChemMedChem* **2009**, *4*, 249−260.

(12) Zulfiqar, F.; Kojima, H.; Nakanishi, M.; Ando, T.; Kitade, Y. *Nucleosides, Nucleotides Nucleic Acids* **2008**, *27*, 1153−1157.

(13) Merino, P.; Tejero, T.; Delso, I. *Curr. Med. Chem.* **2008**, *15*, 954−967.

(14) Goeminne, A.; McNaughton, M.; Bal, G.; Surpateanu, G.; Van der Veken, P.; De Prol, S.; Versees, W.; Steyaert, J.; Haemers, A.; Augustyns, K. *Eur. J. Med. Chem.* **2008**, *43*, 315−326.

(15) Goeminne, A.; Berg, M.; McNaughton, M.; Bal, G.; Surpateanu, G.; Van der Veken, P.; De Prol, S.; Versees, W.; Steyaert, J.; Haemers, A.; Augustyns, K. *Bioorg. Med. Chem.* **2008**, *16*, 6752−6763.

(16) Versees, W.; Goeminne, A.; Berg, M.; Vandemeulebroucke, A.; Haemers, A.; Augustyns, K.; Steyaert, J. *Biochim. Biophys. Acta, Proteins Proteomics* **2009**, *1794*, 953−960.

(17) Lovane, E.; Giabba, B.; Muzzolini, L.; Matafora, V.; Fornili, A.; Minici, C.; Giannese, F.; Degano, M. *Biochemistry* **2008**, *47*, 4418−4426.

(18) Parkin, D. W.; Horenstein, B. A.; Abdulah, D. R.; Estupinan, B.; Schramm, V. L. *J. Biol. Chem.* **1991**, *266*, 20658−20665.

(19) Degano, M.; Gopaul, D. N.; Scapin, G.; Schramm, V. L.; Sacchettini, J. C. *Biochemistry* **1996**, *35*, 5971−5981.

(20) Shi, W. X.; Schramm, V. L.; Almo, S. C. *J. Biol. Chem.* **1999**, *274*, 21114−21120.

(21) Versees, W.; Barlow, J.; Steyaert, J. *J. Mol. Biol.* **2006**, *359*, 331−346.

(22) Parkin, D. W. *J. Biol. Chem.* **1996**, *271*, 21713−21719.

(23) Giabbai, B.; Degano, M. *Structure* **2004**, *12*, 739−749.

(24) Mitterbauer, R.; Karl, T.; Adam, G. *Appl. Environ. Microb.* **2002**, *68*, 1336−1343.

(25) Muzzolini, L.; Versees, W.; Tornaghi, P.; Van Holsbeke, E.; Steyaert, J.; Degano, M. *Biochemistry* **2006**, *45*, 773−782.

(26) Estupinan, B.; Schramm, V. L. *J. Biol. Chem.* **1994**, *269*, 23068−23073.

(27) Miller, R. L.; Sabourin, C. L. K.; Krenitsky, T. A.; Berens, R. L.; Marr, J. J. *J. Biol. Chem.* **1984**, *259*, 5073−5077.

(28) Versees, W.; Loverix, S.; Vandemeulebroucke, A.; Geerlings, P.; Steyaert, J. *J. Mol. Biol.* **2004**, *338*, 1−6.

(29) Vandemeulebroucke, A.; De Vos, S.; Van Holsbeke, E.; Steyaert, J.; Versees, W. *J. Biol. Chem.* **2008**, *283*, 22272−22282.

(30) Vandemeulebroucke, A.; Versees, W.; De Vos, S.; Van Holsbeke, E.; Steyaert, J. *Biochemistry* **2003**, *42*, 12902−12908.

(31) Barlow, J. N.; Steyaert, J. *Biochim. Biophys. Acta, Proteins Proteomics* **2007**, *1774*, 1451−1461.

(32) Vandemeulebroucke, A.; Versees, W.; Steyaert, J.; Barlow, J. N. *Biochemistry* **2006**, *45*, 9307−9318.

(33) Vandemeulebroucke, A.; Minici, C.; Bruno, I.; Muzzolini, L.; Tornaghi, P.; Parkin, D. W.; Versees, W.; Steyaert, J.; Degano, M. *Biochemistry* **2010**, *49*, 8999−9010.

(34) Berti, P. J.; Tanaka, K. S. E. *Adv. Phys. Org. Chem.* **2002**, *37*, 239−314.

(35) Rios-Font, R.; Bertran, J.; Sodupe, M.; Rodriguez-Santiago, L. *Theor. Chem. Acc.* **2011**, *128*, 619−626.

(36) Tiwari, S.; Agnihotri, N.; Mishra, P. C. *J. Phys. Chem. B* **2011**, *115*, 3200−3207.

(37) Mazumder, D.; Kahn, K.; Bruice, T. C. *J. Am. Chem. Soc.* **2002**, *124*, 8825−8833.

(38) Loverix, S.; Geerlings, P.; McNaughton, M.; Augustyns, K.; Vandemeulebroucke, A.; Steyaert, J.; Versees, W. *J. Biol. Chem.* **2005**, *280*, 14799−14802.

(39) Millen, A. L.; Archibald, L. A. B.; Hunter, K. C.; Wetmore, S. D. *J. Phys. Chem. B* **2007**, *111*, 3800−3812.

(40) Przybylski, J. L.; Wetmore, S. D. *J. Phys. Chem. B* **2009**, *113*, 6533−6542.

(41) Millen, A. L.; Wetmore, S. D. *Can. J. Chem.* **2009**, *87*, 850−863.

(42) Chen, Z. Q.; Zhang, C. H.; Xue, Y. *J. Phys. Chem. B* **2009**, *113*, 10409−10420.

(43) Shim, E. J.; Przybylski, J. L.; Wetmore, S. D. *J. Phys. Chem. B* **2010**, *114*, 2319−2326.

(44) Ebrahimi, A.; Habibi-Khorassani, M.; Bazzi, S. *Phys. Chem. Chem. Phys.* **2011**, *13*, 3334−3343.

(45) Sponer, J. E.; Sponer, J.; Fuentes-Cabrera, M. *Chem.—Eur. J.* **2011**, *17*, 847−854.

(46) Mazumder-Shivakumar, D.; Bruice, T. C. *Biochemistry* **2005**, *44*, 7805−7817.

(47) Mazumder, D.; Bruice, T. C. *J. Am. Chem. Soc.* **2002**, *124*, 14591−14600.

(48) Hu, P.; Wang, S.; Zhang, Y. *J. Am. Chem. Soc.* **2008**, *130*, 16721−16728.

(49) Hu, P.; Wang, S.; Zhang, Y. *J. Am. Chem. Soc.* **2008**, *130*, 3806−3813.

(50) Ke, Z.; Guo, H.; Xie, D.; Wang, S.; Zhang, Y. *J. Phys. Chem. B* **2011**, *115*, 3725−3733.

(51) Ke, Z.; Smith, G. K.; Zhang, Y.; Guo, H. *J. Am. Chem. Soc.* **2011**, *133*, 11103−11105.

(52) Ke, Z.; Wang, S.; Xie, D.; Zhang, Y. *J. Phys. Chem. B* **2009**, *113*, 16705−16710.

(53) Ke, Z.; Zhou, Y.; Hu, P.; Wang, S.; Xie, D.; Zhang, Y. *J. Phys. Chem. B* **2009**, *113*, 12750−12758.

(54) Wang, S. L.; Hu, P.; Zhang, Y. K. *J. Phys. Chem. B* **2007**, *111*, 3758−3764.

(55) Zhou, Y.; Wang, S.; Zhang, Y. *J. Phys. Chem. B* **2010**, *114*, 8817−8825.

(56) Zhou, Y.; Zhang, Y. *Chem. Commun.* **2011**, *47*, 1577−1579.

(57) Wu, R. B.; Hu, P.; Wang, S. L.; Cao, Z. X.; Zhang, Y. K. *J. Chem. Theory Comput.* **2010**, *6*, 337−343.

(58) Wu, R. B.; Wang, S. L.; Zhou, N. J.; Cao, Z. X.; Zhang, Y. K. *J. Am. Chem. Soc.* **2010**, *132*, 9471−9479.
(59) Wu, R.; Lu, Z.; Cao, Z.; Zhang, Y. *J. Am. Chem. Soc.* **2011**, *133*, 6110−6113.
(60) Dolinsky, T. J.; Nielsen, J. E.; McCammon, J. A.; Baker, N. A. *Nucleic Acids Res.* **2004**, *32*, W665−W667.
(61) Berendsen, H. J. C.; Postma, J. P. M.; Vangunsteren, W. F.; Dinola, A.; Haak, J. R. *J. Chem. Phys.* **1984**, *81*, 3684−3690.
(62) Cornell, W. D.; Cieplak, P.; Bayly, C. I.; Gould, I. R.; Merz, K. M.; Ferguson, D. M.; Spellmeyer, D. C.; Fox, T.; Caldwell, J. W.; Kollman, P. A. *J. Am. Chem. Soc.* **1995**, *117*, 5179−5197.
(63) Hornak, V.; Abel, R.; Okur, A.; Strockbine, B.; Roitberg, A.; Simmerling, C. *Proteins* **2006**, *65*, 712−725.
(64) Wang, J. M.; Cieplak, P.; Kollman, P. A. *J. Comput. Chem.* **2000**, *21*, 1049−1074.
(65) Jorgensen, W. L.; Chandrasekhar, J.; Madura, J. D.; Impey, R. W.; Klein, M. L. *J. Chem. Phys.* **1983**, *79*, 926−935.
(66) Wang, J. M.; Wolf, R. M.; Caldwell, J. W.; Kollman, P. A.; Case, D. A. *J. Comput. Chem.* **2004**, *25*, 1157−1174.
(67) Frisch, M. J.; Trucks, G. W.; Schlegel, H. B.; Scuseria, G. E.; Robb, M. A.; Cheeseman, J. R.; Montgomery, J. A., Jr.; Vreven, T.; Kudin, K. N.; Burant, J. C.; Millam, J. M.; Iyengar, S. S.; Tomasi, J.; Barone, V.; Mennucci, B.; Cossi, M.; Scalmani, G.; Rega, N.; Petersson, G. A.; Nakatsuji, H.; Hada, M.; Ehara, M.; Toyota, K.; Fukuda, R.; Hasegawa, J.; Ishida, M.; Nakajima, T.; Honda, Y.; Kitao, O.; Nakai, H.; Klene, M.; Li, X.; Knox, J. E.; Hratchian, H. P.; Cross, J. B.; Bakken, V.; Adamo, C.; Jaramillo, J.; Gomperts, R.; Stratmann, R. E.; Yazyev, O.; Austin, A. J.; Cammi, R.; Pomelli, C.; Ochterski, J. W.; Ayala, P. Y.; Morokuma, K.; Voth, G. A.; Salvador, P.; Dannenberg, J. J.; Zakrzewski, V. G.; Dapprich, S.; Daniels, A. D.; Strain, M. C.; Farkas, O.; Malick, D. K.; Rabuck, A. D.; Raghavachari, K.; Foresman, J. B.; Ortiz, J. V.; Cui, Q.; Baboul, A. G.; Clifford, S.; Cioslowski, J.; Stefanov, B. B.; Liu, G.; Liashenko, A.; Piskorz, P.; Komaromi, I.; Martin, R. L.; Fox, D. J.; Keith, T.; Al-Laham, M. A.; Peng, C. Y.; Nanayakkara, A.; Challacombe, M.; Gill, P. M. W.; Johnson, B.; Chen, W.; Wong, M. W.; Gonzalez, C.; Pople, J. A. *Gaussian 03*, revision G03C; Gaussian, Inc.: Wallingford, CT, 2003.
(68) Ryckaert, J. P.; Ciccotti, G.; Berendsen, H. J. C. *J. Comput. Phys.* **1977**, *23*, 327−341.
(69) Zhang, Y. K.; Lee, T. S.; Yang, W. T. *J. Chem. Phys.* **1999**, *110*, 46−54.
(70) Zhang, Y. K. *J. Chem. Phys.* **2005**, *122*, 024114.
(71) Zhang, Y. K. *Theo. Chem. Acc.* **2006**, *116*, 43−50.
(72) Zhang, Y. K.; Liu, H. Y.; Yang, W. T. *J. Chem. Phys.* **2000**, *112*, 3483−3492.
(73) Kumar, S.; Bouzida, D.; Swendsen, R. H.; Kollman, P. A.; Rosenberg, J. M. *J. Comput. Chem.* **1992**, *13*, 1011−1021.
(74) Souaille, M.; Roux, B. *Comput. Phys. Commun.* **2001**, *135*, 40−57.
(75) Beeman, D. *J. Comput. Phys.* **1976**, *20*, 130−139.
(76) Shao, Y.; et al. *Q-Chem*, version 3.0; Q-chem, Inc.: Pittsburgh, PA, 2006.
(77) Ponder, J. W. *TINKER*, Software Tools for Molecular Design, version 4.2; Washington University School of Medicine: St. Louis, MO, 2004.
(78) Cen, Y.; Sauve, A. A. *J. Am. Chem. Soc.* **2010**, *132*, 12286−12298.
(79) Dudev, T.; Lim, C. *J. Am. Chem. Soc.* **2010**, *132*, 16533−16543.
(80) Fahie, K.; Hu, P.; Swatkoski, S.; Cotter, R. J.; Zhang, Y. K.; Wolberger, C. *FEBS J.* **2009**, *276*, 7159−7176.
(81) Liang, Z. J.; Shi, T.; Ouyang, S. S.; Li, H. L.; Yu, K. Q.; Zhu, W. L.; Luo, C.; Jiang, H. L. *J. Phys. Chem. B* **2010**, *114*, 11927−11933.